



Article

Evaluation of Drought Propagation Characteristics and Influencing Factors in an Arid Region of Northeast Asia (ARNA)

Chong Li ¹, Xuan Zhang ^{1,*}, Guodong Yin ¹, Yang Xu ² and Fanghua Hao ¹

¹ Beijing Key Laboratory of Urban Hydrological Cycle and Sponge City Technology, College of Water Sciences, Beijing Normal University, Beijing 100875, China; chong01@mail.bnu.edu.cn (C.L.); 11132018009@bnu.edu.cn (G.Y.); fanghua@bnu.edu.cn (F.H.)

² State Key Laboratory of Hydrosience and Engineering, Department of Hydraulic Engineering, Tsinghua University, Beijing 100084, China; yangx918@tsinghua.edu.cn

* Correspondence: xuan@bnu.edu.cn

Abstract: The characteristics of the drought propagation from meteorological drought (MD) to agricultural drought (AD) differ in various climatic and underlying surface conditions. However, how these factors affect the process of drought propagation is still unclear. In this study, drought propagation and influencing factors were investigated in an arid region of Northeast Asia (ARNA) during 1982–2014. Based on run theory, the drought characteristics were detected using the standardized precipitation index (SPI) and standardized soil moisture index (SMI), respectively. The propagation time from MD to AD was investigated, and the influence factors were identified. Results demonstrated that five clusters (C1–C5) based on land cover distribution were further classified by the K-means cluster algorithm to discuss the spatial and seasonal propagation variation. MD and AD in ARNA became more severe during the study period in all five clusters. The propagation times from MD to AD in all five clusters were shorter (1–3 months) in summer and autumn and longer (5–12 months) in spring and winter. This result suggested that the impact of vegetation on the seasonal drought propagation time was more obvious than that of the spatial drought propagation time. Precipitation and vegetation were the major impactors of AD in spring, summer and autumn ($p < 0.05$). The impact of precipitation on AD was more noticeable in summer, while vegetation mainly influenced AD in spring and autumn. The research also found that drought propagation time had a negative relationship ($p < 0.05$) with precipitation, evapotranspiration, soil moisture and NDVI in this region, which indicated that a rapid hydrological cycle and vegetation can shorten the propagation time from MD to AD. This study can help researchers to understand the drought propagation process and the driving factors to enhance the efficiency of drought forecasting.

Keywords: drought propagation; meteorological drought; agricultural drought; GLDAS; K-means clustering



Citation: Li, C.; Zhang, X.; Yin, G.; Xu, Y.; Hao, F. Evaluation of Drought Propagation Characteristics and Influencing Factors in an Arid Region of Northeast Asia (ARNA). *Remote Sens.* **2022**, *14*, 3307. <https://doi.org/10.3390/rs14143307>

Academic Editor: Won-Ho Nam

Received: 7 June 2022

Accepted: 6 July 2022

Published: 8 July 2022

Publisher's Note: MDPI stays neutral with regard to jurisdictional claims in published maps and institutional affiliations.



Copyright: © 2022 by the authors. Licensee MDPI, Basel, Switzerland. This article is an open access article distributed under the terms and conditions of the Creative Commons Attribution (CC BY) license (<https://creativecommons.org/licenses/by/4.0/>).

1. Introduction

Drought is a natural disaster that results from water deficits. Unlike other natural disasters, such as inundations, long time periods are required for drought development [1,2]. The damages and losses are far-reaching and can affect the social economy, ecological environment, agriculture and drinking water safety [3,4]. In the context of rapid global climate change, drought events become more frequent and persist for longer times, especially in semiarid regions, which aggravates the challenges of the water crisis [5–8].

Drought is commonly categorized into four types, which include meteorological, hydrological, agricultural and socioeconomic droughts [9], and they consist of a lack of water from precipitation, runoff, soil water and social water resources, independently or collectively, respectively [2,10]. Agricultural drought (AD) originating from meteorological drought (MD) [5,11] is commonly described as a shortage in soil moisture that

directly impacts crop growth and plays a vital role in the link between agriculture and ecology [12,13]. AD affects crop production and results in vast damages to agriculture and economies, which can threaten food security and social stability [14,15]. Thus, it is necessary to evaluate drought characteristics and recognize the development of AD, which is of great significance for drought early warning and prevention.

Standardized drought indices are widely used to evaluate drought properties such as frequency, intensity and duration [16–18]. Numerous drought indices have been developed to quantify drought characteristics. For instance, the standardized precipitation index (SPI) [19] and the standardized precipitation and evapotranspiration index (SPEI) [20] are used to evaluate MD, the standardized runoff index (SRI) [21] is used to evaluate hydrological drought, and the standardized soil moisture index (SMI) [22] is employed to assess AD. For example, Yang et al. analyzed the characteristics of hydrological droughts at multiple time scales in the Aksu River Basin using the SRI and found that, with a long time scale, the drought characteristics were more noticeable and that human activities played an important role in hydrological drought [23]. Li et al. studied the relationship between meteorological and hydrological droughts in the Upper Shaying River Basin and concluded that the relationship between meteorological and hydrological droughts had seasonal characteristics [24]. In summary, the SPI and SMI have been widely used due to their flexible time scales and simple calculations [25,26].

Drought propagation is recognized as a transmission process of MD to AD or other drought types [27]. MD is the origin of all types of drought [5]. AD is also delayed relative to MD [11]. Statistics and hydrological models are two basic methods for drought propagation analysis [28], such as the MCC method [2], cross-wavelet analysis [29] and the variable infiltration capacity (VIC) model [30]. Effects of lag, attenuation, pooling and lengthening are common during the process of drought propagation [31,32]. Lag and attenuation are governed by catchment control, and pooling and lengthening are governed by both catchment control and climate control [31]. Drought propagation from MD to AD is affected by climate and underlying surface conditions [33,34]. For example, Li et al. proposed a framework for identifying the drought propagation time with high spatial and temporal resolution from MD to AD. Their results indicated that local water and heat conditions are the main factors for drought propagation times [35]. Huang et al. examined the impact of potential surface property factors on drought propagation and found that land cover has potential impacts on drought propagation from MD to AD [34]. The mechanisms of the impact of climatic and underlying surface factors on drought development and propagation are complex and still unclear. Recent studies stress that it is necessary to further analyze the factors influencing the drought propagation process.

Land cover is one of the most important underlying surface factors, and the water consumption capacities of varying land cover types and stages of vegetation growth are different and significantly impact drought propagation [33,36]. The impacts of vegetation on drought propagation can be achieved by two approaches. One is comparing the vegetation characteristics of subbasins or subregions, which is an effective method [30]. The other uses hydrological models that can simulate the process of the hydrological cycle [37]. However, the limitations of the hydrological model used on a large scale lead to more uncertainties [30]. Land cover is significantly disturbed by human activities, which makes it difficult to exactly detect the impacts of vegetation on drought propagation. Most previous studies are devoted to evaluating drought propagation properties and comparing their variations in different land cover types. However, research on the comprehensive influence of both the spatial and seasonal properties of land cover on drought propagation is still scarce. Therefore, the spatial and seasonal influences of land cover on the drought propagation process need to be further investigated.

The ARNA is located in Northeastern Asia and is a semiarid area. Existing studies show that drought in the study area has become more serious in recent decades [38,39]. The ARNA has fewer human settlements and weak human activities [40,41], and land cover plays a central role in drought propagation and can explain the effects of vegetation

on drought propagation. In addition, the land cover of the ARNA has spatial cluster characteristics, which can be used to effectively investigate the impact of vegetation on drought propagation. This is the reason that the ARNA was selected.

This study aims to explore the response of drought propagation to climatic and underlying surface factors. We also consider the effects of vegetation on drought propagation, both on spatial and seasonal scales. This study uses the SPI and SMI to investigate drought propagation from MD to AD and to evaluate the effects of driving factors on the drought propagation process. Therefore, the objectives of this study are (1) to assess the characteristics of drought propagation from MD to AD; and (2) to estimate the effects of influence factors on the drought propagation process from MD to AD.

2. Materials and Methods

2.1. Study Area

The ARNA, with a total area of 648,739 km², is located in Northeastern Asia, 42.54–53.44°N and 104.97–122.88°E, and spreads across three countries: China, Russia and Mongolia (Figure 1). Hulun Lake is China's fifth-largest inland lake and is located in the ARNA, with an area of 2058 km² [41]. There are three major rivers in the ARNA. The Kherlen River and Wuerxun River are located upstream of Hulun Lake, while the Argun River is located downstream of Hulun Lake. The ARNA is a semiarid area that has a temperate continental monsoon climate. The average annual temperature is approximately 0 °C, and the average annual precipitation is 290 mm, most of which occurs in summer [40,42]. ARNA is a relatively natural ecosystem with few human activities [40,41]. Drought has frequently occurred and has been exacerbated in the past 30 years in the ARNA [38,39]. The ecosystems of the ARNA are generally fragile and more sensitive to drought events. Grassland, forest and bareland are the main land cover types. Spatial heterogeneities of land cover explain that the underlying surface conditions of the ARNA are different, which significantly affects the drought propagation process.

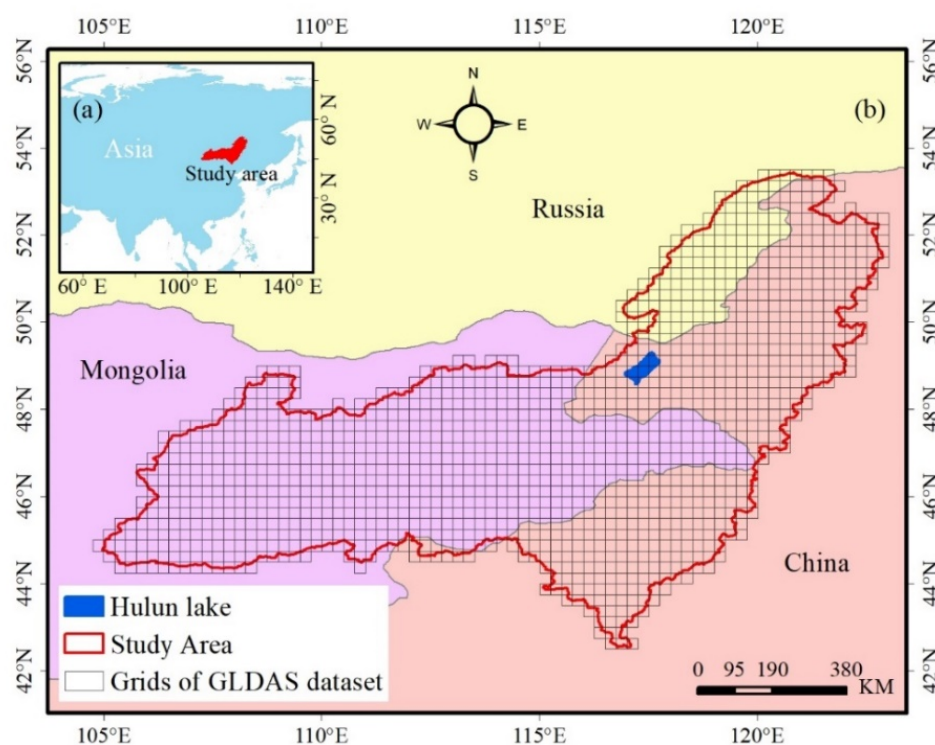


Figure 1. General location of the study area. (a) Location of the ARNA in Asia and (b) geographic details of the ARNA.

2.2. Data

The Global Land Data Assimilation System data version 2 (GLDAS-2.0) was acquired from NASA (<https://disc.gsfc.nasa.gov/> (accessed on 26 June 2021)). GLDAS is a global grid dataset with a spatial resolution of 0.25° that is widely applied to evaluate environmental issues [43–45], such as drought monitoring [26] and drought propagation [46,47]. To prove the reliability of the data, we compared the GLDAS data with another dataset that is widely used, the climate data of the CRU TS (Climatic Research Unit gridded Time Series) dataset [48]. The performance is shown in Appendix A, Figure A1. Specifically, the monthly precipitation, evapotranspiration and soil moisture data from the GLDAS dataset with 1391 grids from 1982 to 2014 were employed to calculate the SPI and SMI and the influence factors on drought propagation time that were used in this study. Land cover data with a spatial resolution of 300 m were obtained from NTPDC (<https://data.tpdc.ac.cn/en/> (accessed on 13 November 2021)). Land cover data were adopted to assess the drought propagation characteristics at varying land cover percentage levels. Due to land cover change on spatial grids having significant influences on drought propagation, which could have impacted the following research, referencing a previous study [49], this study considered that there was no alteration in land cover types from 1982 to 2014. Forest, grassland and bareland were selected in this study according to the land cover spatial map. Specifically, the grids with 0.25° resolution were basic evaluating units. For each basic evaluating unit, the land cover percentage of the forest, grassland and bareland was calculated because the land cover data had a 300 m resolution, which is far less than that of basic units. Digital elevation model (DEM) data were obtained from the GTOPO30 dataset of the U.S. Geological Survey (USGS) (<https://www.usgs.gov/centers/eros/science/usgs-eros-archive-digital-elevation-global-30-arc-second-elevation-gtopo30> (accessed on 24 July 2019)). GTOPO30 is a global DEM dataset with a 1 km spatial resolution. The DEM was resampled to fit a 0.25° spatial resolution by using ArcGIS. The DEM was used to investigate the underlying surface characteristics and to analyze its effects on drought propagation. The normalized difference vegetation index (NDVI) was acquired from the Global Inventory Modelling and Mapping Studies (GIMMS) (<https://ecocast.arc.nasa.gov/data/pub/gimms/3g.v1/> (accessed on 23 July 2018)). The spatial resolution of this dataset was $1/12^\circ$ (approximately 8 km). This study used the NDVI to explore the spatial distribution pattern and the influence of vegetation on drought propagation without NDVI trend analysis. To match the resolution of the climate data, the NDVI data were resampled to a 0.25° resolution.

2.3. Methods

This study aimed to evaluate the effects of driving factors on drought propagation from MD to AD. Seasonal and spatial drought propagation processes were analyzed, supported by K-means clustering, drought indices, run theory and Pearson correlation methods. The methodological framework for this work included four steps. Step 1 was data collection and preprocessing. Step 2 was spatial cluster calculation. According to the percentage of dominant land cover types, the spatial clusters of the study area were identified by K-means clusters. Step 3 involved the computation of drought indices and propagation times. Gamma distribution was used to determine the drought index series. Then, run theory was used to detect drought events and characteristics based on drought series. The Pearson correlation method was used to identify the drought propagation time from MD to AD. Step 4 was influence factor analysis. This step included the response of AD of climatic and vegetation and the impactors on drought propagation. The findings of these analyses were supported by the Pearson correlation method. Figure 2 presents the flowchart of this study. The introduction of the key methods is presented in the following subsections.

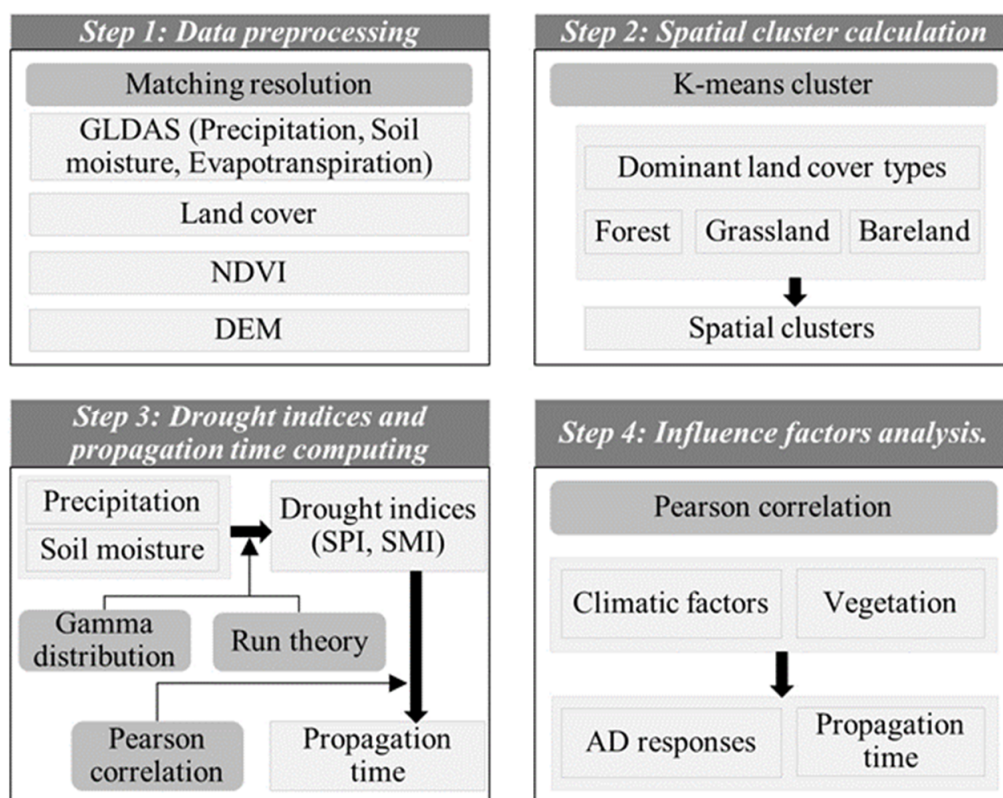


Figure 2. Flowchart of this study.

2.3.1. K-Means Cluster Analysis

The percentage of dominant land cover types at each grid was selected as a controlling factor to analyze the aggregation characteristics of the underlying surface. The K-means cluster method is an unsupervised machine learning algorithm that is widely used for clustering problems [50–52] because it is an easy application to use and has high efficiency and excellent performance [53]. The K-means cluster splits numerous data points into K clusters and K coherent centers based on specific characteristics [54], which causes the lengths of the internal points among each cluster to be small as possible, while causing the lengths between clusters to be as large as possible. K-means clustering is controlled by minimizing the objective function (Equations (1) and (2)), and the aim is that the sum of the square error, S , is the minimum value. For the specific calculation steps for the K-means cluster, see the references [54–56].

$$S = \sum_{i=1}^k \sum_{x \in C_i} \|x - h_i\|_2^2 \quad (1)$$

$$h_i = \frac{1}{|C_i|} \sum_{x \in C_i} x \quad (2)$$

where S is the sum of squares error (Euclidean distance) between the elements in each cluster and the cluster center, x is the sample data point, h is the cluster center, C_i is the i th cluster, and k is the number of clusters.

2.3.2. Drought Indices and Drought Characteristics

In this study, standardized drought indices SPI [19] and SMI [22] were adopted to evaluate meteorological and agricultural droughts, respectively. SPI and SMI are simple to calculate, flexible on time scales and widely used in MD and AD monitoring and evaluation. The SPI and SMI are calculated by precipitation and soil moisture series, respectively, during

a certain accumulating period. Generally, the SPI and SMI are determined by fitting gamma distributions with monthly precipitation and soil moisture data [57,58]. A two-parameter gamma probability distribution function was employed to fit accumulated precipitation and soil moisture using the following Equation (3):

$$h(x) = \frac{1}{\beta^\lambda \Gamma(\lambda)} x^{\lambda-1} e^{-\frac{x}{\beta}}, x > 0 \quad (3)$$

where x is the value of precipitation or soil moisture accumulation; λ and β denote the shape and scale parameters of the gamma distribution, respectively. $\Gamma(\lambda)$ is the gamma function, which can be described as Equation (4):

$$\Gamma(\lambda) = \int_0^\infty x^{\lambda-1} e^{-x} dx \quad (4)$$

The maximum likelihood estimation method can be used to estimate the parameters λ and β (Equation (5)):

$$\lambda = \frac{1}{4A} \left(1 + \sqrt{1 + \frac{4A}{3}} \right), \beta = \frac{\bar{x}}{\lambda}, \text{ with } A = \lg(\bar{x}) - \frac{\sum_{i=1}^n \lg(\bar{x})}{n} \quad (5)$$

where n is the number of data series.

To fully assess drought characteristics, multiple time scale indices should be used. This study evaluates drought under monthly, seasonal and annual time scales, where the corresponding drought indices are SPI-1, -3, -12 and SMI-1, -3, -12, respectively.

Based on standardized drought indices SPI and SMI, the events of meteorological and agricultural drought were detected by run theory [59]. When the value of the drought index series was less than a threshold value, the run was identified as a drought event. The threshold value was set as -0.5 according to the Chinese national standard grades of meteorological drought (GB/T 20481-2017) and previous studies [60]. Drought duration (DD), drought intensity (DI) and drought frequency (DF) were identified to describe the drought characteristics. The DD value is determined by the months of continued drought events, in which a higher number of months indicates longer DDs. The DI is the average value of the drought index for each drought event. The smaller the DI value is, the more serious the drought events are. DF is the average annual number of drought events for the study period, and the DF values are higher with more frequent droughts. Specific descriptions of these drought characteristics can be found in previous studies [23,61–63]. The formulas of the drought characteristics can be expressed as follows (Equations (6)–(8)):

$$DD = t_2 - t_1 + 1 \quad (6)$$

$$DI = \frac{\sum_{t=t_1}^{t_2} S(t)}{DD} \quad (7)$$

$$DF = \frac{N}{n_{year}} \quad (8)$$

where t_2 and t_1 are the times of drought onset and ending, respectively. $S(t)$ is the value of SPI or SMI in the monthly time t , N is the number of drought events during the study period, and n_{year} is the number of years of the study stage.

2.3.3. Investigation of Drought Propagation Definition and Influence Factors

In general, AD is triggered by MD and experiences a certain delay time from MD. The certain time is recognized as the drought propagation time from MD to AD. Correlation analysis has become a popular method to acquire drought propagation time. This study employed Pearson correlation coefficients to investigate the relationships between the SPI and SMI at varying time scales and to identify the propagation time from MD to

AD. The maximum correlation coefficient (MCC) between SPI- n ($n = 1, 2, 3, \dots, 12$) and SMI-1 can express the most appropriate SPI accumulation period. The SPI- n can assess the precipitation deficit in the last n months. The n is defined as the propagation time from MD to AD [37]. The equation for the Pearson correlation coefficient is shown below (Equation (9)):

$$R_{xy} = \frac{\sum_{i=1}^n (x_i - \bar{x})(y_i - \bar{y})}{\sqrt{\sum_{i=1}^n (x_i - \bar{x})^2 \sum_{i=1}^n (y_i - \bar{y})^2}} \quad (9)$$

where R_{xy} denotes the Pearson correlation between x and y , and \bar{x} and \bar{y} represent the average values of x and y , respectively. n denotes the number of each variable. The range of R_{xy} is -1 to 1 . When the value approaches -1 or 1 , this indicates a more negative or positive correlation. When the value is 0 , there is no correlation.

Many factors have significant impacts on the process of drought propagation [29]. This study focused on hydrology and underlying surface conditions, including precipitation, evapotranspiration, soil moisture and NDVI. The approach that compares the characteristics of these factors in different regions is effective [64]. The characteristics of drought propagation and influence factors were analyzed in different seasons and clusters. Finally, the relationship between drought propagation time and influence factors was concluded.

3. Results

3.1. Cluster Results Analysis

Land cover types affect the spatial drought propagation process. Land cover has spatial clustering characteristics in the ARNA (Figure 3a). The grasslands are widely distributed in the study area, forests are located in the northeast of the ARNA, and bareland is located in the southwest of the ARNA. There are also some areas with forest grass mixing and grass bare mixing in the ARNA. Therefore, five clusters were determined. To avoid the uncertainty of subjective classification, the objective method of K-means cluster analysis was adopted to categorize all grids according to the percentage of the forest, grassland and bareland at each grid. A spatial map of the cluster distributions is shown in Figure 3b. The spatial distribution of clusters is consistent with that of land cover. Cluster 1 (C1) and Cluster 2 (C) are located in the northeast of the ARNA, Cluster 3 (C3) is distributed mainly in the center of the ARNA, and Cluster 4 (C4) and Cluster 5 (C5) are located in the southwest of the ARNA. Figure 3c shows the properties of land cover and cluster centers. The results revealed that C1 is dominated by forest, C2 is dominated by forest and grassland, C3 is dominated by grassland, C4 is dominated by grassland and bareland, and bareland is the main land cover type of C5.

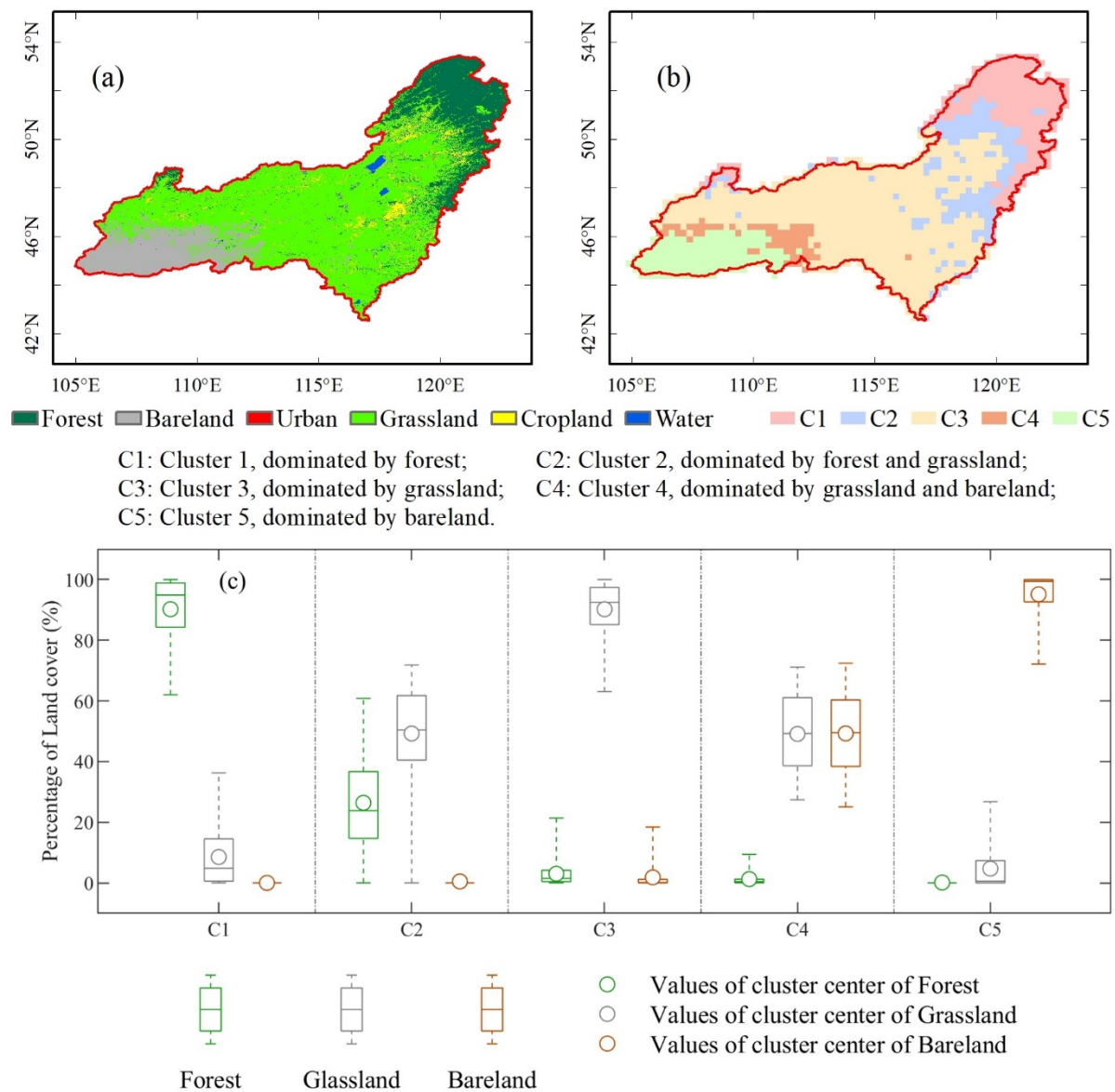


Figure 3. Land cover properties and results of cluster analysis: (a) land cover map, (b) spatial distribution of clusters and (c) percentage and cluster centers of the forest, grassland and bareland.

3.2. Meteorological and Underlying Surface Condition Analysis

Hydrological and underlying surface factors, including NDVI, DEM, precipitation and soil moisture, were analyzed because these factors affect the propagation process (Figure 4). The precipitation and soil moisture in most areas of the ARNA were below 400 mm and 25 mm, respectively, indicating that the study area is a typical dry region. From the east to the west of the ARNA, the elevation increased; the NDVI, precipitation and soil moisture decreased. The changes in DEM, precipitation and soil moisture are notable from C1 to C5. With the vegetation coverage declining from the east to the west of the ARNA, the elevation had an increasing trend, and the NDVI, precipitation and soil moisture had a decreasing trend. When the area had higher vegetation coverage (C1), the median values of NDVI, DEM, precipitation and soil moisture were 0.47, 866 m, 443.58 mm and 22.73 mm, respectively. This condition, with relatively abundant water resources, can promote vegetation growth. However, the higher water consumption of forests can affect the drought propagation process. For the area with less vegetation (C4 and C5), the median values of NDVI, DEM, precipitation and soil moisture in C4 and C5 were 0.15 and 0.11,

1084 and 1150 m, 174.58 and 135.74 mm and 12.63 and 12.62 mm, respectively. The DEM was higher and the NDVI, precipitation and soil moisture were lower in this condition, which limits vegetation growth (Figure 4c,d).

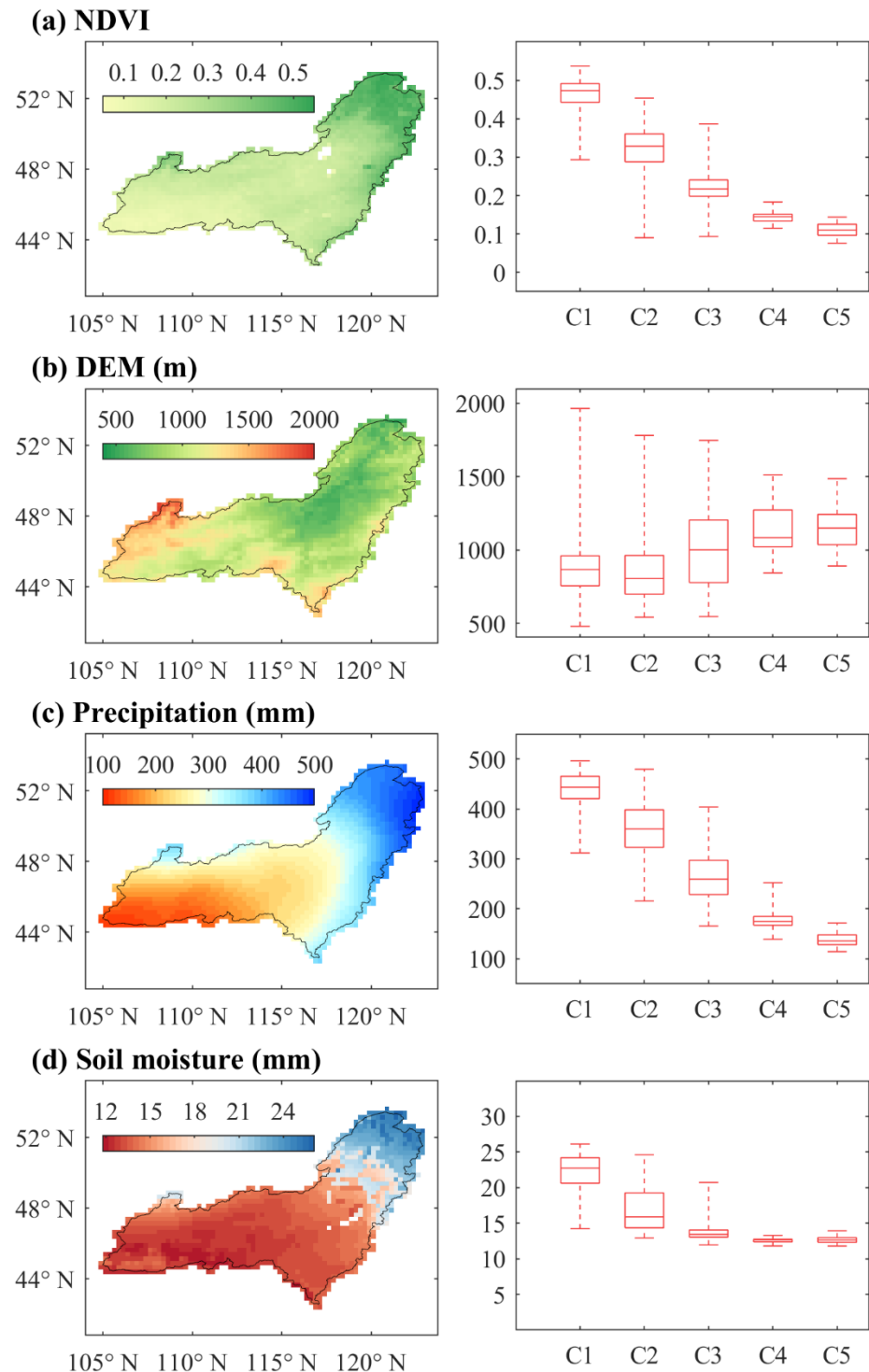


Figure 4. Spatial distribution and boxplot in different clusters of NDVI (a), DEM (b), precipitation (c) and soil moisture (d).

3.3. Drought Characteristics Analysis

To detect the episodes of drought, the changes in the series of SPI-1, -3, -12 and SMI-1, -3 and -12 in C1 to C5 were determined and are shown in Figure 5. Drought episodes

were identified in the study period, in which the ARNA experienced severe drought in approximately 1987 and 2015. Drought episodes were prolonged with increasing time scale. For SPI, five clusters provided a slight change, indicating that MD presented weak spatial discrepancies (Figure 5a–e), although that the MD in C2 and C4 was more severe than that in other clusters in 1988. The drought event that began in 2005 had a longer duration in the ARNA. These findings correspond to existing research that found that the drought in Mongolia became more serious from 1982 to 2014 [38,39]. For SMI, the AD change is evidenced through the alteration of the SMI series (Figure 5f–j). From 1982 to 2000, the ARNA was relatively wet. However, a drought event was identified to occur in 1986 under C2 and C4. Extremely dry episodes were detected in approximately 2005 in the ARNA. There were fewer differences among the five clusters. However, the time of drought occurrence in C5 was ahead of that in other clusters. Drought propagation effects with lag, attenuation, pooling and lengthening were obvious in the ARNA, which may have been caused by catchment factors such as vegetation [32].

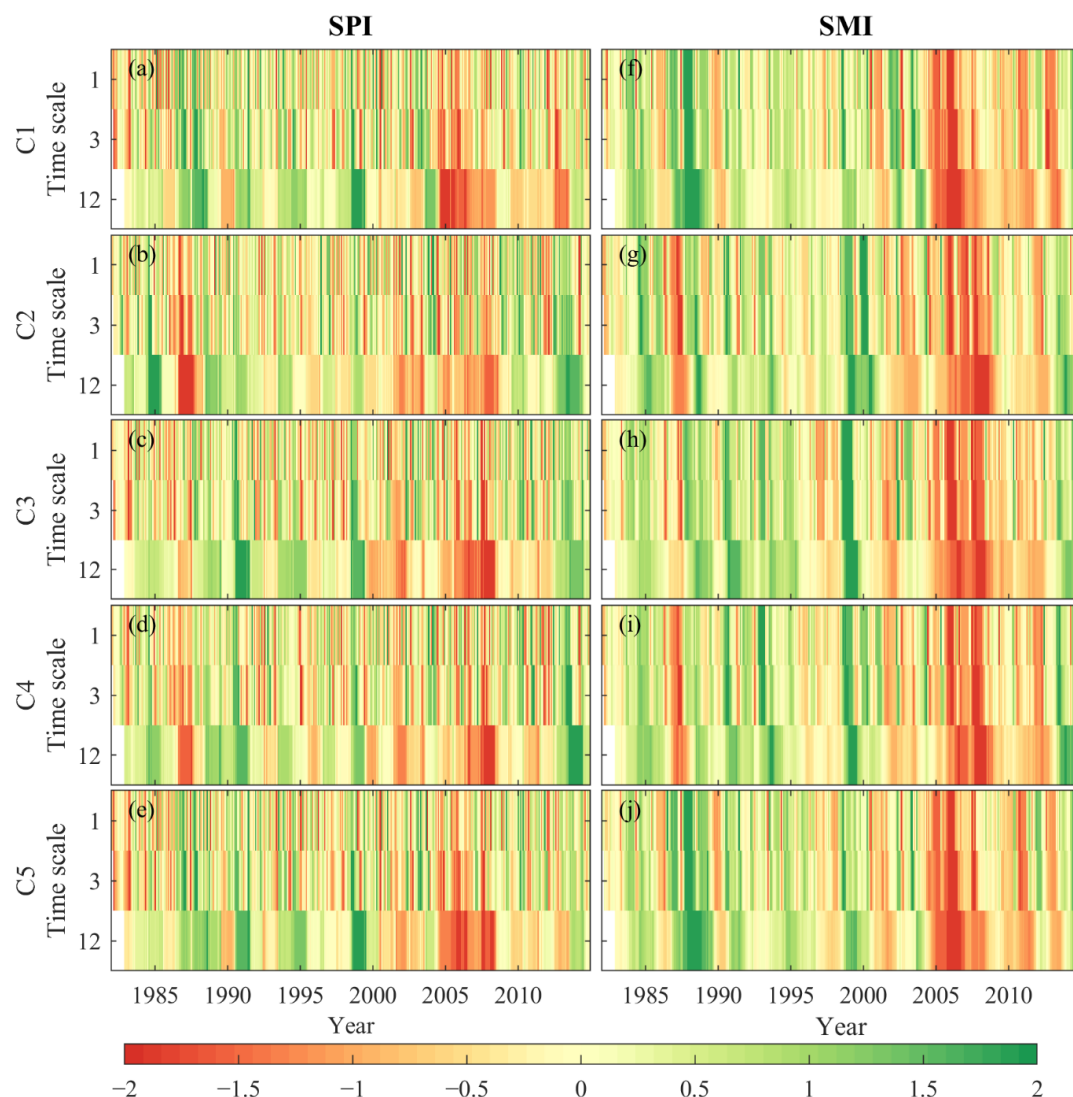


Figure 5. Variation of time series of SPI (a–e) and SMI (f–j) values at -1, -3 and -12 month time scales in five clusters.

Figure 6 presents drought characteristics for the five clusters according to the SPI and SMI at -1, -3 and -12 month time scales during 1982–2014. The average DD of AD was larger than that of MD in all clusters except C2 and C5 at the 12-month time scale, whose maximum value of DD was larger than that of MD (Figure 6a,b). The longest average DDs

for SPI -1, -3 and -12 were in C4 (3.43 months), in C4 (5.91 months) and in C5 (23.88 months), respectively, while the longest average DDs for SRI -1, -3 and -12 were 7.52 months (C4), 9.09 months (C4) and 32 months (C4), respectively. The DDs for SPI -1, -3 and -12 were more serious than those for SRI -1, -3 and -12 in all clusters (Figure 6c,d). The most severe average DI values for SPI -1, -3 and -12 were -0.8 (C1), -0.71 (C3) and -0.60 (C4), respectively, and those for SRI -1, -3 and -12 were -0.72 (C5), -0.56 (C5) and -0.52 (C2), respectively. The DFs for SPI -1, -3 and -12 were more frequent than those for SRI -1, -3 and -12, except in C2 and C5 at the 12-month scale (Figure 6e,f). The maximum DFs for SPI -1, -3 and -12 were 1.97 (C1, C5), 1.24 (C5) and 0.39 (C1) times/year, respectively, and those for SRI -1, -3 and -12 were 0.91 (C1, C3), 0.79 (C2) and 0.3 (C5) times/year, respectively. Generally, AD had a longer DD, a weaker intensity and more frequent drought events than MD in the ARNA. The average values of drought characteristics were relatively stable, with fewer spatial changes across all five clusters. This is mainly because drought is determined by deficits in water, especially precipitation and soil moisture. Despite obvious discrepancies existing among the five clusters, the ARNA is located in an arid area with the same water condition [37], and the annual precipitation and soil moisture in most areas were below 400 mm and 25 mm, respectively (Figure 4). However, MD is significantly influenced by surface conditions such as land cover change and vegetation growth, which affects drought propagation [34].

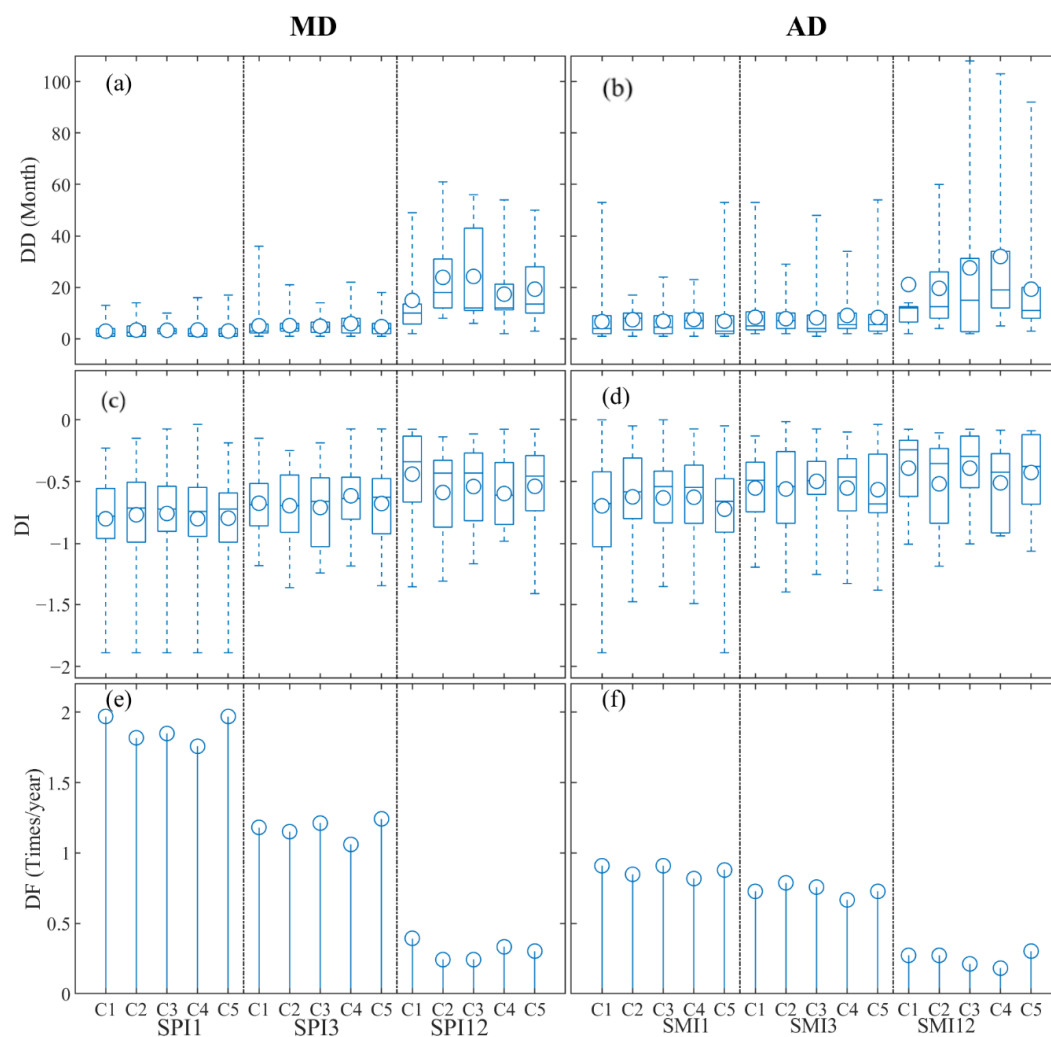


Figure 6. Drought characteristics at -1, -3 and -12 month time scales based on SPI and SRI for five clusters in the ARNA. (a) DD of MD, (b) DD of AD, (c) DI of MD, (d) DI of AD, (e) DF of MD and (f) DF of AD.

3.4. Drought Propagation from MD to AD

The seasonal Pearson correlation coefficients between the SPI- n and SMI-1 were computed in five clusters to explore the most likely cumulative relationship between MD and AD. As shown in Figure 7A, the correlation between the SPI- n and SMI was high and had evident seasonality. There were fewer spatial discrepancies between C1 and C5. The correlation coefficient in summer was higher than that in other seasons. In spring and winter, the correlation coefficients were relatively low. Similarly, the drought propagation time had similar characteristics to the correlation coefficients between the SPI- n and SMI-1. The propagation time was identified by the MCC between SPI- n and SMI-1. The MCC can state the most probable SPI accumulation stage, and n is the propagation time. The most likely seasonal propagation time from MD to AD in the five clusters is presented in Figure 7B. The drought propagation time in the five clusters was characterized by obvious seasonality. In summer and autumn, drought quickly propagated from MD to AD with 1–3 month propagation times. Drought propagation was slow in spring and winter, with 5–12 month propagation times. Varying from C1 to C5, the drought propagation time had fewer discrepancies in the same season, except in winter under C5. The land cover type is different from C1 to C5, and the land cover growth has differences over the four seasons. Therefore, the results indicated that the effects of vegetation on seasonal drought propagation may be larger than that of regional drought propagation in the ARNA.

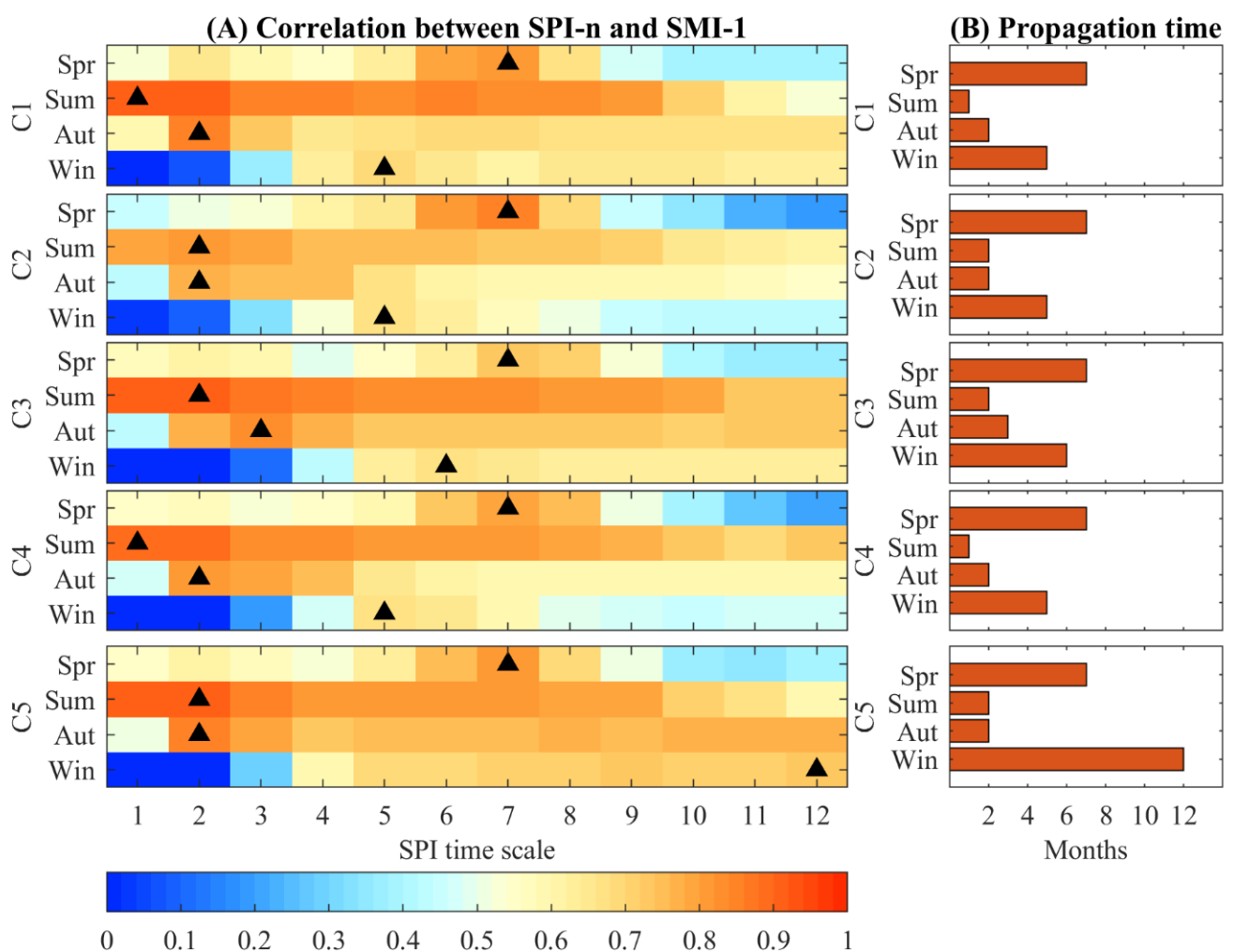


Figure 7. Drought propagation characteristics from MD to AD. (A) The correlation of SPI- n and SMI during the spring, summer, autumn and winter in five clusters. The black triangle indicates the MCC. (B) Propagation time in four seasons for each cluster.

These alterations were determined by the differences in meteorological conditions and underlying vegetation [30,65]. Summer and autumn are rainy seasons and have rapid hydrological cycle processes. Strong precipitation and evapotranspiration result in rapid changes in soil moisture, which is the main reason that summer has a strong relationship and a short drought propagation time. In the dry seasons of spring and winter, due to the low temperature and weak evapotranspiration, the hydrological cycle slowed down. In addition, the study area experiences a frozen period in winter, and precipitation does not supply soil moisture. These reasons may extend the time from MD to AD in winter and spring. Vegetation also plays an important role in drought propagation. In summer, vegetations have a relatively large leaf area, which accelerates the loss of soil moisture. In winter, vegetations slow down soil moisture loss due to low evapotranspiration. Previous studies pointed out that the vegetation type has a significant influence on drought propagation [33,66]; however, there are fewer discrepancies in drought propagation among C1 to C5 in the ARNA. The key reason is that the ARNA is an arid area with low annual precipitation and soil moisture.

4. Discussion

4.1. The Response of AD to Climate and Vegetation

Soil moisture can characterize the degree of AD; with a deficit in soil moisture, the AD is more serious. Soil moisture is also the link between precipitation and vegetation. To explore the relationship between AD and climate and vegetation, the Pearson correlation coefficients between soil moisture and precipitation and NDVI in different seasons under the five clusters were discussed (Figure 8). The impact of precipitation on AD is more obvious in summer, and vegetation mainly impacts AD in spring and autumn. Soil moisture has a significant ($p < 0.05$) positive relationship with precipitation and NDVI in spring, summer and autumn, indicating that the increases in precipitation and vegetation growth in the wet season accelerate water transport, which will affect the process of drought propagation [37,67]. In addition, as the vegetation grows, the water consumption increases because the vegetation needs to obtain more soil moisture [68]. In spring and autumn, the correlation coefficient of soil moisture and precipitation (approximately ranging from 0.40 to 0.56) was lower than that of soil moisture and NDVI (approximately ranging from 0.60 to 0.93). The precipitation at these times is lower than that in summer, while the NDVI at these times is higher than that in winter. The results showed that the contribution to the drought propagation process by vegetation was larger than that by precipitation in spring and autumn [69]. The correlation coefficient was weak in winter and was controlled by soil freezing. In winter, precipitation does not enter the soil, and soil water cannot be absorbed by vegetation due to soil freezing [70]. There are fewer discrepancies in the correlation coefficient in the five clusters. The key reason is that the ARNA is located in an arid area, and the annual precipitation and the soil moisture in most regions of the ARNA are below 400 mm and 25 mm, respectively. This decisive condition determines that the propagation characteristics are similar [57].

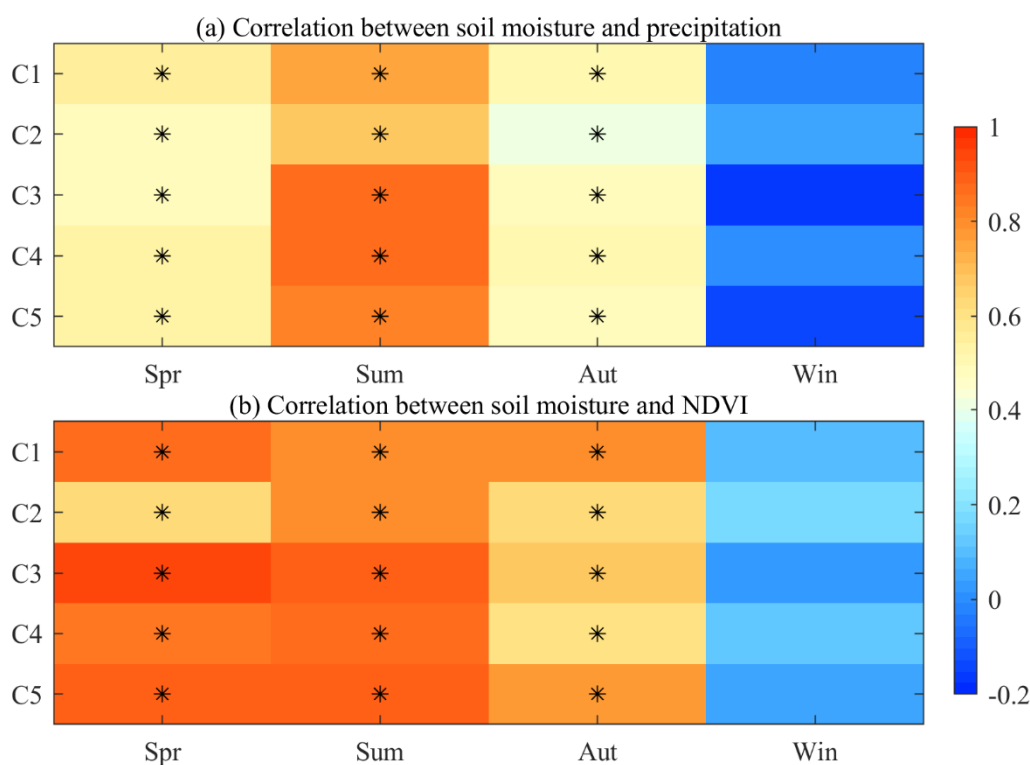


Figure 8. The correlation coefficients between soil moisture and precipitation (a) and NDVI (b) in spring, summer, autumn and winter in the five clusters. * indicates significance at the 0.05 level.

4.2. Impactors of Drought Propagation

The impact of precipitation and vegetation on the seasonal drought propagation time is more significant than that on the regional drought propagation time. Figure 7A shows a highly positive correlation between MD and AD. The main reason for this is that MD and AD are tightly connected by hydrometeorological conditions, and AD originates from MD [5,11]. The results indicated that the drought propagation times varied in different seasons but changed less in various clusters (Figure 7B). In addition, drought propagation could be impacted by meteorological conditions, soil properties and vegetation cover [29,57,71]. The elevation determines the local moisture conditions and vegetation growth in the monsoon region and affects the values of precipitation and soil moisture [72,73]. The water consumption of vegetation affects the process of drought propagation. In the ARNA, although the annual precipitation of C1–C5 varied significantly, the amounts of most positions were below 400 mm (Figure 4), which is characteristic of an arid area. Due to precipitation being a basic factor for drought development [37], the spatial propagation time from MD to AD had fewer discrepancies despite the land cover having obvious alterations. Seasonal precipitation and vegetation changes contribute to the propagation process and account for the changes in propagation time. Previous studies also show that the drought propagation process from MD to AD may be affected by climate and vegetation [65,74]. For example, Huang et al. found that the evapotranspiration rate can accelerate drought propagation [69]. Zhou et al. investigated the relationship among drought indices and concluded that forest and other land cover types significantly affected the process from MD to AD [75]. Specifically, vegetation can consume and can acquire much water from the soil, which demonstrates that vegetation can impact the process from MD to AD [36,68]. Therefore, the effects of climate and vegetation on drought propagation need to be further discussed.

This study attempted to detect the influencing factors on drought propagation according to the changes in climate factors, vegetation and propagation time. The relationship between propagation time and influence factors is shown in Figure 9. It can be seen that

precipitation, evapotranspiration, soil moisture and NDVI are the most important factors in drought propagation and significantly ($p < 0.05$) affect the drought propagation time, with the values of these factors changing in opposite directions. For climatic factors, precipitation, evapotranspiration and soil moisture are relatively higher in wet seasons, especially in summer. The hydrological process is accelerated and further shortens the response time from MD to AD. The propagation time becomes shorter. In dry seasons, due to the decrease in temperature and precipitation, evapotranspiration is low, which further slows the hydrological process and prolongs the drought propagation time [65,69,76]. For vegetation factors, the annual changes in NDVI are similar to climatic factors. Vegetation evapotranspiration consumes water in the soil, especially in growing seasons that exceed the drought propagation times [1,77]. These results can verify that the drought propagation time is short in the growing season, with a quick hydrological cycle speed and well-growing vegetation.

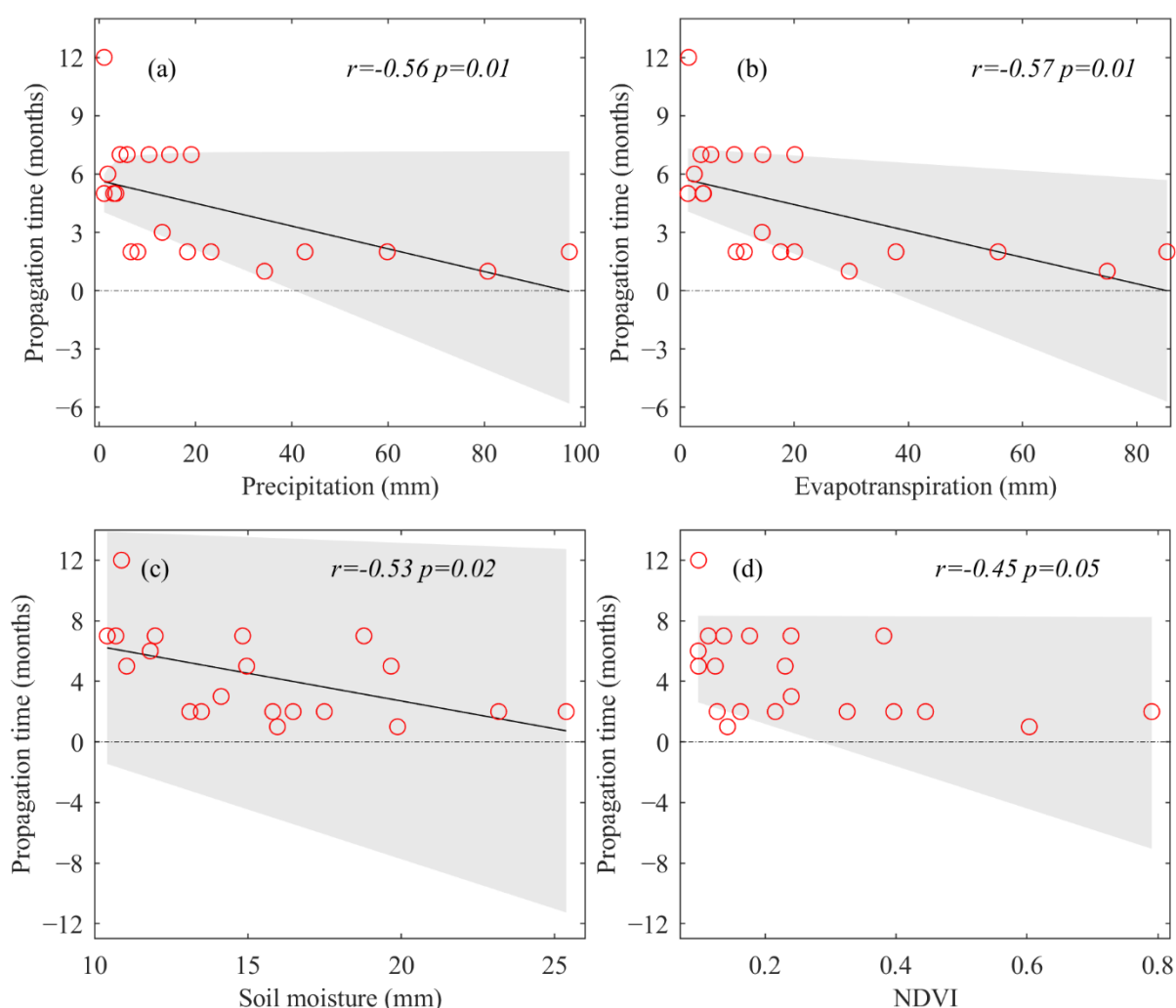


Figure 9. The relationship between seasonal propagation time and hydrometeorological factors (precipitation (a), evapotranspiration (b) and soil moisture (c)) and underlying surface factors (NDVI (d)).

4.3. Limitations and Prospects

Although climate and vegetation factors had obvious variation across the ARNA (Figure 4), the propagation times had slight alterations (Figure 7B). There were two reasons for these results. One reason is that the ARNA is a typical arid area with less precipitation, which causes fewer spatial discrepancies in propagation time [37]. The other reason is that the monthly MCC method is simple and is helpful to recognize in the propagation process,

but there are still some limitations to understanding the propagation process on a more specific time scale [35]. We will determine the drought propagation time from MD to AD on a 2-week or weekly time scale. Due to the restrictions of observational data of precipitation and soil water data, this study acquired these datasets from the GLDAS product, whose performance may lead to uncertainties in the evaluation results [13]. We will use more datasets to sufficiently analyze drought assessments in the future. In addition, we explored the impact of climate and vegetation factors on drought propagation from MD to AD and concluded that vegetation has an important influence on the drought propagation process. Therefore, we will specifically investigate the relationship between the vegetation growth process and the drought propagation process and select more useful drought and vegetation indices, such as SPEI and gross primary productivity (GPP) [78].

5. Conclusions

This study primarily investigated the properties of drought propagation from MD to AD and its driving factors in the ARNA, using the K-means clustering method, during 1982–2014. First, five clusters were detected by K-means clustering based on the dominant vegetation cover. Then, drought characteristics were identified according to drought indices and run theory. Finally, the seasonal characteristics of drought propagation and its driving factors were discussed in the five clusters. The main conclusions of this study are as follows.

Five clusters (C1–C5) were detected by the K-means cluster algorithm with different characteristics of land cover. From 1982 to 2014, the drought condition in the ARNA gradually became more severe in all five clusters. MD and AD were detected by the SPI and SRI. AD had a longer DD, a weaker intensity and more frequent drought events than MD in the ARNA. Drought characteristics had little spatial variation across all five clusters.

The impact of vegetation on the seasonal drought propagation time is larger than that on the regional drought propagation time. The correlation between SPI- n and SMI-1 is higher in summer and autumn and lower in winter and spring. Drought propagation times in all five clusters were 1–3 months in summer and autumn and 5–12 months in spring and winter.

The response of AD to precipitation is more obvious during summer, while vegetation mainly affects AD in spring and autumn. Precipitation and vegetation have a close relationship with soil moisture in spring, summer and autumn ($p < 0.05$). The correlation coefficient between soil moisture and NDVI (approximately 0.60–0.93) was higher than that between soil moisture and precipitation (approximately 0.40–0.56) in spring and autumn.

Drought propagation time from MD to AD has a significant ($p < 0.05$) negative relationship with precipitation, evapotranspiration, soil moisture and NDVI. This result indicates that the rapid hydrological cycle and well-growing vegetation can accelerate the water transport process and further shorten the propagation time from MD to AD.

These conclusions might help in understanding the drought propagation process from MD to AD and can provide scientific reference for addressing drought disasters.

Author Contributions: Conceptualization, C.L. and X.Z.; methodology, C.L., X.Z. and Y.X.; data curation, C.L. and G.Y.; formal analysis, C.L. and X.Z.; writing—original draft preparation, C.L.; writing—review and editing, C.L. and X.Z.; visualization, C.L., Y.X. and F.H.; supervision, X.Z. and F.H.; funding acquisition, X.Z. and G.Y. All authors have read and agreed to the published version of the manuscript.

Funding: This research was funded by the National Key Research and Development Program of China (Grant No. 2019YFC0409201) and the National Natural Science Foundation of China (Grant No. 41907157).

Data Availability Statement: Not applicable.

Conflicts of Interest: The authors declare no conflict of interest.

Appendix A

To prove the reliability of the data, the GLDAS data were compared with another widely used set of climate data, the CRU TS (Climatic Research Unit gridded Time Series) dataset. The CRU TS, with 0.5° spatial resolution, was principally developed by the UK's Natural Environment Research Council (NERC) and the US Department of Energy. We mainly considered the variable of monthly precipitation. Due to the discrepancies in spatial resolution, 1040 grids in two datasets around the study area were selected, respectively. To evaluate the prediction performance, the Nash–Sutcliffe efficiency coefficient (NSE) and root mean square error (RMSE) were used in this study. Higher NSE and lower RMSE values indicate better prediction performance. The results are shown in Figure A1. Results indicated that all selected grids had an average value of 8.98 mm for RMSE, and an average value of 0.92 for NSE, indicating that the GLDAS data have high quality, similar to the CRU TS data, and are reliable.

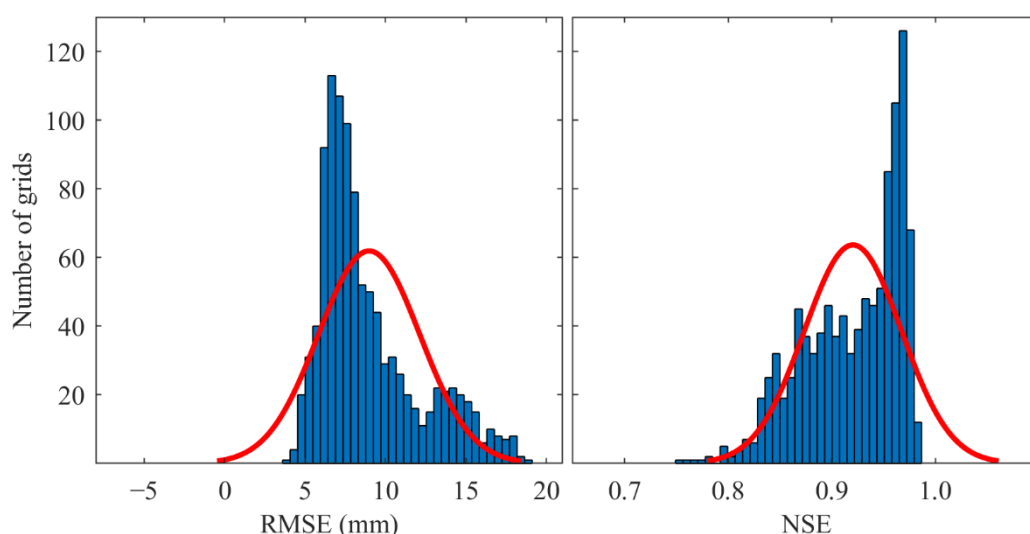


Figure A1. The performance of GLDAS data and CRU TS data.

References

- Mishra, A.K.; Singh, V.P. A review of drought concepts. *J. Hydrol.* **2010**, *391*, 202–216. [\[CrossRef\]](#)
- Ding, Y.; Gong, X.; Xing, Z.; Cai, H.; Zhou, Z.; Zhang, D.; Sun, P.; Shi, H. Attribution of meteorological, hydrological and agricultural drought propagation in different climatic regions of China. *Agric. Water Manag.* **2021**, *255*, 106996. [\[CrossRef\]](#)
- Song, X.; Gao, X.; Wu, P.; Zhao, X.; Zhang, W.; Zou, Y.; Siddique, K.H.M. Drought responses of profile plant-available water and fine-root distributions in apple (*Malus pumila* Mill.) orchards in a loessial, semi-arid, hilly area of China. *Sci. Total Environ.* **2020**, *723*, 137739. [\[CrossRef\]](#)
- Wang, L.; Yu, H.; Yang, M.; Yang, R.; Gao, R.; Wang, Y. A drought index: The standardized precipitation evapotranspiration runoff index. *J. Hydrol.* **2019**, *571*, 651–668. [\[CrossRef\]](#)
- Hao, Z.; Singh, V.P. Drought characterization from a multivariate perspective: A review. *J. Hydrol.* **2015**, *527*, 668–678. [\[CrossRef\]](#)
- Li, Y.; Lu, H.; Yang, K.; Wang, W.; Tang, Q.; Khem, S.; Yang, F.; Huang, Y. Meteorological and hydrological droughts in Mekong River Basin and surrounding areas under climate change. *J. Hydrol. Reg. Stud.* **2021**, *36*, 100873. [\[CrossRef\]](#)
- Li, L.; Song, X.; Xia, L.; Fu, N.; Feng, D.; Li, H.; Li, Y. Modelling the effects of climate change on transpiration and evaporation in natural and constructed grasslands in the semi-arid Loess Plateau, China. *Agric. Ecosyst. Environ.* **2020**, *302*, 107077. [\[CrossRef\]](#)
- Dai, A.; Trenberth, K.E.; Qian, T. A Global Dataset of Palmer Drought Severity Index for 1870–2002: Relationship with Soil Moisture and Effects of Surface Warming. *J. Hydrometeorol.* **2004**, *5*, 1117–1130. [\[CrossRef\]](#)
- Wilhite, D.A.; Glantz, M.H. Understanding: The Drought Phenomenon: The Role of Definitions. *Water Int.* **1985**, *10*, 111–120. [\[CrossRef\]](#)
- Gu, L.; Chen, J.; Yin, J.; Xu, C.-Y.; Chen, H. Drought hazard transferability from meteorological to hydrological propagation. *J. Hydrol.* **2020**, *585*, 124761. [\[CrossRef\]](#)
- Heim, R.R., Jr. A Review of Twentieth-Century Drought Indices Used in the United States. *Bull. Am. Meteorol. Soc.* **2002**, *83*, 1149–1166. [\[CrossRef\]](#)
- Huang, S.; Wang, L.; Wang, H.; Huang, Q.; Leng, G.; Fang, W.; Zhang, Y. Spatio-temporal characteristics of drought structure across China using an integrated drought index. *Agric. Water Manag.* **2019**, *218*, 182–192. [\[CrossRef\]](#)

13. Zhang, Y.; Hao, Z.; Feng, S.; Zhang, X.; Xu, Y.; Hao, F. Agricultural drought prediction in China based on drought propagation and large-scale drivers. *Agric. Water Manag.* **2021**, *255*, 107028. [[CrossRef](#)]
14. Martínez-Fernández, J.; González-Zamora, A.; Sánchez, N.; Gumuzzio, A.; Herrero-Jiménez, C.M. Satellite soil moisture for agricultural drought monitoring: Assessment of the SMOS derived Soil Water Deficit Index. *Remote Sens. Environ.* **2016**, *177*, 277–286. [[CrossRef](#)]
15. Hao, Z.; Singh, V.P.; Xia, Y. Seasonal Drought Prediction: Advances, Challenges, and Future Prospects. *Rev. Geophys.* **2018**, *56*, 108–141. [[CrossRef](#)]
16. Jiang, R.; Xie, J.; He, H.; Luo, J.; Zhu, J. Use of four drought indices for evaluating drought characteristics under climate change in Shaanxi, China: 1951–2012. *Nat. Hazards* **2015**, *75*, 2885–2903. [[CrossRef](#)]
17. Muhammad, W.; Muhammad, S.; Khan, N.M.; Si, C. Hydrological drought indexing approach in response to climate and anthropogenic activities. *Theor. Appl. Climatol.* **2020**, *141*, 1401–1413. [[CrossRef](#)]
18. Zheng, Y.; Zhang, X.; Yu, J.; Xu, Y.; Wang, Q.; Li, C.; Yao, X. Assessing the Joint Impact of Climatic Variables on Meteorological Drought Using Machine Learning. *Front. Earth Sci.* **2022**, *10*, 835142. [[CrossRef](#)]
19. McKee, T.; Doesken, N.; Kliest, J. The relationship of drought frequency and duration to time scales. In Proceedings of the Eighth Conference on Applied Climatology, American Meteorological Society, Anaheim, CA, USA, 17–23 January 1993.
20. Vicente-Serrano, S.M.; Beguería, S.; López-Moreno, J.I. A Multiscalar Drought Index Sensitive to Global Warming: The Standardized Precipitation Evapotranspiration Index. *J. Clim.* **2010**, *23*, 1696–1718. [[CrossRef](#)]
21. Shukla, S.; Wood, A.W. Use of a standardized runoff index for characterizing hydrologic drought. *Geophys. Res. Lett.* **2008**, *35*, L02405. [[CrossRef](#)]
22. Hao, Z.; AghaKouchak, A. A Nonparametric Multivariate Multi-Index Drought Monitoring Framework. *J. Hydrometeorol.* **2014**, *15*, 89–101. [[CrossRef](#)]
23. Yang, P.; Xia, J.; Zhang, Y.; Zhan, C.; Cai, W.; Zhang, S.; Wang, W. Quantitative study on characteristics of hydrological drought in arid area of Northwest China under changing environment. *J. Hydrol.* **2021**, *597*, 126343. [[CrossRef](#)]
24. Li, Q.; He, P.; He, Y.; Han, X.; Zeng, T.; Lu, G.; Wang, H. Investigation to the relation between meteorological drought and hydrological drought in the upper Shaying River Basin using wavelet analysis. *Atmos. Res.* **2020**, *234*, 104743. [[CrossRef](#)]
25. Zhao, L.; Lyu, A.; Wu, J.; Hayes, M.; Tang, Z.; He, B.; Liu, J.; Liu, M. Impact of meteorological drought on streamflow drought in Jinghe River Basin of China. *Chin. Geogr. Sci.* **2014**, *24*, 694–705. [[CrossRef](#)]
26. Hao, Z.; AghaKouchak, A.; Nakhjiri, N.; Farahmand, A. Global integrated drought monitoring and prediction system. *Sci. Data* **2014**, *1*, 140001. [[CrossRef](#)]
27. Elfatih, A.B.E.; Yeh, P.J.-F. On the asymmetric response of aquifer water level to floods and droughts in Illinois. *Water Resour. Res.* **1999**, *35*, 1199–1217. [[CrossRef](#)]
28. Apurv, T.; Sivapalan, M.; Cai, X. Understanding the Role of Climate Characteristics in Drought Propagation. *Water Resour. Res.* **2017**, *53*, 9304–9329. [[CrossRef](#)]
29. Huang, S.; Li, P.; Huang, Q.; Leng, G.; Hou, B.; Ma, L. The propagation from meteorological to hydrological drought and its potential influence factors. *J. Hydrol.* **2017**, *547*, 184–195. [[CrossRef](#)]
30. Zhang, T.; Su, X.; Zhang, G.; Wu, H.; Wang, G.; Chu, J. Evaluation of the impacts of human activities on propagation from meteorological drought to hydrological drought in the Weihe River Basin, China. *Sci. Total Environ.* **2022**, *819*, 153030. [[CrossRef](#)]
31. Van Loon, A.F. Hydrological drought explained. *WIREs Water* **2015**, *2*, 359–392. [[CrossRef](#)]
32. Zhang, X.; Hao, Z.; Singh, V.P.; Zhang, Y.; Feng, S.; Xu, Y.; Hao, F. Drought propagation under global warming: Characteristics, approaches, processes, and controlling factors. *Sci. Total Environ.* **2022**, *838*, 156021. [[CrossRef](#)]
33. Van Lanen, H.A.J.; Wanders, N.; Tallaksen, L.M.; Van Loon, A.F. Hydrological drought across the world: Impact of climate and physical catchment structure. *Hydrol. Earth Syst. Sci.* **2013**, *17*, 1715–1732. [[CrossRef](#)]
34. Huang, S.; Huang, Q.; Chang, J.; Leng, G.; Xing, L. The response of agricultural drought to meteorological drought and the influencing factors: A case study in the Wei River Basin, China. *Agric. Water Manag.* **2015**, *159*, 45–54. [[CrossRef](#)]
35. Li, Y.; Huang, S.; Wang, H.; Zheng, X.; Huang, Q.; Deng, M.; Peng, J. High-resolution propagation time from meteorological to agricultural drought at multiple levels and spatiotemporal scales. *Agric. Water Manag.* **2022**, *262*, 107428. [[CrossRef](#)]
36. Peña-Angulo, D.; Vicente-Serrano, S.M.; Domínguez-Castro, F.; Noguera, I.; Tomas-Burguera, M.; López-Moreno, J.I.; Lorenzo-Lacruz, J.; El Kenawy, A. Unravelling the role of vegetation on the different trends between climatic and hydrologic drought in headwater catchments of Spain. *Anthropocene* **2021**, *36*, 100309. [[CrossRef](#)]
37. Wu, J.; Miao, C.; Zheng, H.; Duan, Q.; Lei, X.; Li, H. Meteorological and Hydrological Drought on the Loess Plateau, China: Evolutionary Characteristics, Impact, and Propagation. *J. Geophys. Res. Atmos.* **2018**, *123*, 11569–11584. [[CrossRef](#)]
38. Tong, S.; Lai, Q.; Zhang, J.; Bao, Y.; Lusi, A.; Ma, Q.; Li, X.; Zhang, F. Spatiotemporal drought variability on the Mongolian Plateau from 1980–2014 based on the SPEI-PM, intensity analysis and Hurst exponent. *Sci. Total Environ.* **2018**, *615*, 1557–1565. [[CrossRef](#)]
39. Narisu, N.; Bao, Y.; Yushan, B. Drought Temporal Variation Characteristics Analysis based on the PDSI Data in Mongolian Plateau. In *Advances in Intelligent Systems Research, Proceedings of the 7th Annual Meeting of Risk Analysis Council of China Association for Disaster Prevention (RAC-2016), Changsha, China, 4–6 November 2016*; Atlantis Press: Amsterdam, The Netherlands, 2016; pp. 844–849. [[CrossRef](#)]
40. Cai, Z.; Jin, T.; Li, C.; Offerdinger, U.; Zhang, S.; Ding, A.; Li, J. Is China’s fifth-largest inland lake to dry-up? Incorporated hydrological and satellite-based methods for forecasting Hulun lake water levels. *Adv. Water Resour.* **2016**, *94*, 185–199. [[CrossRef](#)]

41. Cao, Y.; Fu, C.; Wang, X.; Dong, L.; Yao, S.; Xue, B.; Wu, H.; Wu, H. Decoding the dramatic hundred-year water level variations of a typical great lake in semi-arid region of northeastern Asia. *Sci. Total Environ.* **2021**, *770*, 145353. [[CrossRef](#)]
42. Fan, C.; Song, C.; Liu, K.; Ke, L.; Xue, B.; Chen, T.; Fu, C.; Cheng, J. Century-Scale Reconstruction of Water Storage Changes of the Largest Lake in the Inner Mongolia Plateau Using a Machine Learning Approach. *Water Resour. Res.* **2021**, *57*, e2020WR028831. [[CrossRef](#)]
43. Rodell, M.; Houser, P.R.; Jambor, U.; Gottschalck, J.; Mitchell, K.; Meng, C.-J.; Arsenault, K.; Cosgrove, B.; Radakovich, J.; Bosilovich, M.; et al. The Global Land Data Assimilation System. *Bull. Am. Meteorol. Soc.* **2004**, *85*, 381–394. [[CrossRef](#)]
44. Min, X.; Shangguan, Y.; Huang, J.; Wang, H.; Shi, Z. Relative Strengths Recognition of Nine Mainstream Satellite-Based Soil Moisture Products at the Global Scale. *Remote Sens.* **2022**, *14*, 2739. [[CrossRef](#)]
45. Ming, W.; Ji, X.; Zhang, M.; Li, Y.; Liu, C.; Wang, Y.; Li, J. A Hybrid Triple Collocation-Deep Learning Approach for Improving Soil Moisture Estimation from Satellite and Model-Based Data. *Remote Sens.* **2022**, *14*, 1744. [[CrossRef](#)]
46. Zhu, Y.; Liu, Y.; Wang, W.; Singh, V.P.; Ren, L. A global perspective on the probability of propagation of drought: From meteorological to soil moisture. *J. Hydrol.* **2021**, *603*, 126907. [[CrossRef](#)]
47. Chen, N.; Li, R.; Zhang, X.; Yang, C.; Wang, X.; Zeng, L.; Tang, S.; Wang, W.; Li, D.; Niyogi, D. Drought propagation in Northern China Plain: A comparative analysis of GLDAS and MERRA-2 datasets. *J. Hydrol.* **2020**, *588*, 125026. [[CrossRef](#)]
48. Harris, I.; Osborn, T.J.; Jones, P.; Lister, D. Version 4 of the CRU TS monthly high-resolution gridded multivariate climate dataset. *Sci. Data* **2020**, *7*, 109. [[CrossRef](#)]
49. Ding, Y.; Xu, J.; Wang, X.; Peng, X.; Cai, H. Spatial and temporal effects of drought on Chinese vegetation under different coverage levels. *Sci. Total Environ.* **2020**, *716*, 137166. [[CrossRef](#)]
50. Choudhury, A.; Dutta, D.; Bera, D.; Kundu, A. Regional variation of drought parameters and long-term trends over India using standardized precipitation evapotranspiration index. *J. Environ. Manag.* **2021**, *296*, 113056. [[CrossRef](#)]
51. Santos, J.F.; Pulido-Calvo, I.; Portela, M.M. Spatial and temporal variability of droughts in Portugal. *Water Resour. Res.* **2010**, *46*, W03503. [[CrossRef](#)]
52. Yang, Y.; Gan, T.Y.; Tan, X. Spatiotemporal changes of drought characteristics and their dynamic drivers in Canada. *Atmos. Res.* **2020**, *232*, 104695. [[CrossRef](#)]
53. Macqueen, J. Some methods for classification and analysis of multivariate observations. In *Proceedings of the Fifth Berkeley Symposium on Mathematical Statistics and Probability: Weather Modification*; University of California Press: Berkeley, CA, USA, 1967.
54. Fooladi, M.; Golmohammadi, M.H.; Safavi, H.R.; Singh, V.P. Fusion-based framework for meteorological drought modeling using remotely sensed datasets under climate change scenarios: Resilience, vulnerability, and frequency analysis. *J. Environ. Manag.* **2021**, *297*, 113283. [[CrossRef](#)] [[PubMed](#)]
55. Jing, J.; Ke, S.; Li, T.; Wang, T. Energy method of geophysical logging lithology based on K-means dynamic clustering analysis. *Environ. Technol. Innov.* **2021**, *23*, 101534. [[CrossRef](#)]
56. Xu, H.; Ma, C.; Lian, J.; Xu, K.; Chaima, E. Urban flooding risk assessment based on an integrated k-means cluster algorithm and improved entropy weight method in the region of Haikou, China. *J. Hydrol.* **2018**, *563*, 975–986. [[CrossRef](#)]
57. Xu, Y.; Zhang, X.; Hao, Z.; Singh, V.P.; Hao, F. Characterization of agricultural drought propagation over China based on bivariate probabilistic quantification. *J. Hydrol.* **2021**, *598*, 126194. [[CrossRef](#)]
58. Angelidis, P.; Maris, F.; Kotsovinos, N.; Hrissanthou, V. Computation of Drought Index SPI with Alternative Distribution Functions. *Water Resour. Manag.* **2012**, *26*, 2453–2473. [[CrossRef](#)]
59. Yevjevich, V. Objective Approach to Definitions and Investigations of Continental Hydrologic Droughts, An. Ph.D. Thesis, Colorado State University, Fort Collins, CO, USA, 1967.
60. Yao, N.; Li, Y.; Lei, T.; Peng, L. Drought evolution, severity and trends in mainland China over 1961–2013. *Sci. Total Environ.* **2018**, *616–617*, 73–89. [[CrossRef](#)]
61. Guo, H.; Bao, A.; Liu, T.; Jiapaer, G.; Ndayisaba, F.; Jiang, L.; Kurban, A.; Maeyer, P.D. Spatial and temporal characteristics of droughts in Central Asia during 1966–2015. *Sci. Total Environ.* **2018**, *624*, 1523–1538. [[CrossRef](#)] [[PubMed](#)]
62. Zhai, J.; Mondal, S.K.; Fischer, T.; Wang, Y.; Su, B.; Huang, J.; Tao, H.; Wang, G.; Ullah, W.; Uddin, M.J. Future drought characteristics through a multi-model ensemble from CMIP6 over South Asia. *Atmos. Res.* **2020**, *246*, 105111. [[CrossRef](#)]
63. Wang, T.; Tu, X.; Singh, V.P.; Chen, X.; Lin, K. Global data assessment and analysis of drought characteristics based on CMIP6. *J. Hydrol.* **2021**, *596*, 126091. [[CrossRef](#)]
64. Van Loon, A.F.; Rangelcroft, S.; Coxon, G.; Breña Naranjo, J.A.; Van Ogtrop, F.; Van Lanen, H.A.J. Using paired catchments to quantify the human influence on hydrological droughts. *Hydrol. Earth Syst. Sci.* **2019**, *23*, 1725–1739. [[CrossRef](#)]
65. Xu, Y.; Zhang, X.; Wang, X.; Hao, Z.; Singh, V.P.; Hao, F. Propagation from meteorological drought to hydrological drought under the impact of human activities: A case study in northern China. *J. Hydrol.* **2019**, *579*, 124147. [[CrossRef](#)]
66. Van Dijk, A.I.J.M.; Beck, H.E.; Crosbie, R.S.; Jeu, R.A.M.D.; Liu, Y.Y.; Podger, G.M.; Timbal, B.; Viney, N.R. The Millennium Drought in southeast Australia (2001–2009): Natural and human causes and implications for water resources, ecosystems, economy, and society. *Water Resour. Res.* **2013**, *49*, 1040–1057. [[CrossRef](#)]
67. Yang, Y.; Shang, S.; Jiang, L. Remote sensing temporal and spatial patterns of evapotranspiration and the responses to water management in a large irrigation district of North China. *Agric. For. Meteorol.* **2012**, *164*, 112–122. [[CrossRef](#)]
68. Wang, Y.; Fu, B.; Liu, Y.; Li, Y.; Feng, X.; Wang, S. Response of vegetation to drought in the Tibetan Plateau: Elevation differentiation and the dominant factors. *Agric. For. Meteorol.* **2021**, *306*, 108468. [[CrossRef](#)]

69. Han, Z.; Huang, S.; Huang, Q.; Leng, G.; Wang, H.; Bai, Q.; Zhao, J.; Ma, L.; Wang, L.; Du, M. Propagation dynamics from meteorological to groundwater drought and their possible influence factors. *J. Hydrol.* **2019**, *578*, 124102. [[CrossRef](#)]
70. Frauenfeld, O.W.; Zhang, T.; Barry, R.G.; Gilichinsky, D. Interdecadal changes in seasonal freeze and thaw depths in Russia. *J. Geophys. Res. Atmos.* **2004**, *109*, D05101. [[CrossRef](#)]
71. Gevaert, A.I.; Veldkamp, T.I.E.; Ward, P.J. The effect of climate type on timescales of drought propagation in an ensemble of global hydrological models. *Hydrol. Earth Syst. Sci.* **2018**, *22*, 4649–4665. [[CrossRef](#)]
72. Li, H.; Li, Y.; Shen, W.; Li, Y.; Lin, J.; Lu, X.; Xu, X.; Jiang, J. Elevation-Dependent Vegetation Greening of the Yarlung Zangbo River Basin in the Southern Tibetan Plateau, 1999–2013. *Remote Sens.* **2015**, *7*, 16672–16687. [[CrossRef](#)]
73. Yao, J.; Yang, Q.; Mao, W.; Zhao, Y.; Xu, X. Precipitation trend–Elevation relationship in arid regions of the China. *Glob. Planet. Chang.* **2016**, *143*, 1–9. [[CrossRef](#)]
74. Van Loon, A.F.; Tjiedeman, E.; Wanders, N.; van Lanen, H.A.J.; Teuling, A.J.; Uijlenhoet, R. How climate seasonality modifies drought duration and deficit. *J. Geophys. Res. Atmos.* **2014**, *119*, 4640–4656. [[CrossRef](#)]
75. Zhou, K.; Li, J.; Zhang, T.; Kang, A. The use of combined soil moisture data to characterize agricultural drought conditions and the relationship among different drought types in China. *Agric. Water Manag.* **2021**, *243*, 106479. [[CrossRef](#)]
76. Teuling, A.J.; Van Loon, A.F.; Seneviratne, S.I.; Lehner, I.; Aubinet, M.; Heinesch, B.; Bernhofer, C.; Grünwald, T.; Prasse, H.; Spank, U. Evapotranspiration amplifies European summer drought. *Geophys. Res. Lett.* **2013**, *40*, 2071–2075. [[CrossRef](#)]
77. Yinglan, A.; Wang, G.; Liu, T.; Shrestha, S.; Xue, B.; Tan, Z. Vertical variations of soil water and its controlling factors based on the structural equation model in a semi-arid grassland. *Sci. Total Environ.* **2019**, *691*, 1016–1026. [[CrossRef](#)]
78. Liu, Q.; Zhang, J.; Zhang, H.; Yao, F.; Bai, Y.; Zhang, S.; Meng, X.; Liu, Q. Evaluating the performance of eight drought indices for capturing soil moisture dynamics in various vegetation regions over China. *Sci. Total Environ.* **2021**, *789*, 147803. [[CrossRef](#)]